PAPER • **OPEN ACCESS**

Trajectory-dependent highly charged ion-induced electron yield from single-layer graphene

To cite this article: A Niggas *et al* 2025 *Phys. Scr.* **100** 015403

Physica Scripta

PAPER

Trajectory-dependent highly charged ion-induced electron yield from single-layer graphene

A Niggas, F Aumayr and R A Wilhelm
TU Wien, Institute of Applied Physics, Vienna, EU, Austria
E-mail: anna@iap.tuwien.ac.at

Keywords: highly charged ions, electron emission, neutralisation dynamics

OPEN ACCESS

RECEIVED
13 September 2024

REVISED
5 November 2024

ACCEPTED FOR PUBLICATION
19 November 2024

PUBLISHED
2 December 2024

Abstract

We study the neutralisation dynamics of highly charged ions by transmission through a free-standing single layer of graphene in dependence of the particle trajectory. Both the secondary electron yield and the neutralisation of the ion increase for increasing scattering angles (smaller impact parameters). This supports the current understanding of highly charged ion deexcitation, according to which the presence of an interatomic deexcitation mechanism with improved efficiency in the proximity of neighbours is necessary in addition to intraatomic radiative- and non-radiative decay pathways.

1. Introduction

Highly charged ions (HCIs) are an exotic, yet intriguing type of particles [1]. By removing electrons from an initially neutral atom, the particle builds up a potential energy corresponding to the sum of binding energies of the missing electrons. As the binding energy increases with every additional ionised electron, the potential energy can reach several tens to hundreds of keV for heavy atomic ions [2]. This feature sets ions apart from other particles, like electrons and photons, where solely a (kinetic) energy can be controlled. For ions, different charge states and corresponding electron configurations offer a variety of applications. For instance, open 4*d*-subshell transitions in (highly charged) tin plasmas are responsible for the renowned 13.5 nm extreme-ultraviolet (EUV) light emission used in state-of-the-art nanolithography [3–5] and magnetic dipole transitions are the basis for high-accuracy optical atomic clocks [6, 7].

Additional effects come into play when HCIs are not considered on their own but in interaction with other particles [8, 9] or surfaces [10–12]. In the latter, HCIs can lead to surface nanostructures, where the amount of excited material depends strongly on the kinetic and potential energy of the projectile [13–15]. While swift ions have a long range in a bulk sample, for slow highly charged ions, i.e. velocities smaller than the Bohr velocity $v_0 = 2.18 \cdot 10^6$ m/s, the damage is limited to the very first surface layers. This surface sensitivity is governed by the deposition of the potential energy, which was found in the 1990s to be ultrafast in grazing scattering and transmission experiments through thin foils [16–18]. However, resultant neutralisation times within femtoseconds could not be explained using solely radiative and non-radiative decay.

The emergence of two-dimensional (2D) materials allowed for a better 'resolution' of charge exchange studies (one material layer rather than several nm) [19, 20] and led to new insights into the deexcitation mechanisms involved: Wilhelm *et al* [21] proposed that the interatomic Coulombic decay (ICD) is the dominating process in the HCI deexcitation. This two-centre Auger-Meitner process is distance dependent ($\sim 1/r^6$) and has rates on the order of $\sim 10^{15}\ s^{-1}$ [22]. A characteristic of this process is the emission of many low-energy electrons, which could be confirmed for HCI transmission through graphene [23]. Also, a scattering angle dependence of HCI neutralisation was discussed by Lemell *et al* [24] and Creutzburg *et al* [25] - a clear indication of the contribution of material atoms to the deexcitation processes.

In this work, we take this approach one step further and additionally measure the electron emission yield from a free-standing single layer of graphene upon transmission of Xe^{30+} ions in dependence of the scattering

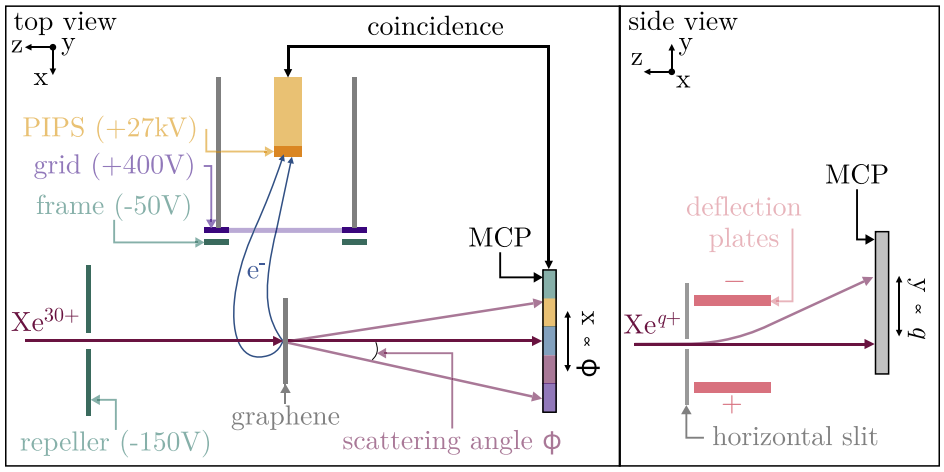

Figure 1. Schematic of the used experimental setup: top view (left) and side view (right). Ions transmitted through a 2D sample, here, graphene, impinge on a position-sensitive multichannel plate (MCP) detector. Thanks to a horizontal slit placed after the sample and in front of a pair of deflection plates we use the two axes of the MCP to detect the ion scattering angle ($x \propto \phi$) and charge state ($y \propto q$) after transmission. For electron number statistics, we use a grid to attract electrons towards a passivated implanted planar silicon (PIPS) detector; negatively biased repeller and frame electrodes help guide the electrons towards the grid. The schematic is not to scale.

angle. An increasing yield with increasing scattering angle is also found for the secondary electrons and also suggests a dependence of the neutralisation dynamics on the impact parameter.

2. Methods

A Dreebit electron beam ion source (EBIS-A) is employed to produce Xe ions in charge states up to $q = 40$ with kinetic energies up to 10 keV $\times q$. Using a Wien filter, we select a single charge state, here $q = 30$, to enter the target chamber where the ion beam is shaped and focused onto a freestanding single-layer of graphene (SLG). The samples are commercially acquired from Graphenea [26] and cleaned according to the thermal treatment described in [27] before ion irradiation.

After interacting with the 2D layer, our setup is used to study (1) the ion after transmission and (2) the mean number of emitted electrons per incident ion. The setup is described in detail in literature [28, 29] and briefly introduced below.

Ions transmitted through the sample are guided towards a position-sensitive multichannel plate (MCP) detector with RoentDek [30] timing electronics. To use both axes of the MCP for detection of different physical quantities, we insert a horizontal slit and a parallel pair of deflection plates immediately afterwards. Therewith, we can study the ion scattering angle ϕ along the horizontal (x-)axis and the exit charge state q_{out} of the ions (after interaction) on the vertical (y-)axis. The latter gives access to the neutralisation dynamics of the projectile with regard to the number of captured electrons $n_{\mathrm{e}} = q - q_{\mathrm{out}}$. The MCP can also be used to monitor the initial beam width, which translates to an angular width of $<0.1°$. Furthermore, using an independent electrostatic energy analyzer we determine a width of <7 eV $\times q$ of the initial energy profile of the ion beam. Figure 1 schematically depicts the geometry of our experiment.

In addition to the projectile after interaction, we collect the electrons emitted from the graphene layer due to the ion impact. For that purpose, we employ an electron statistics setup as described in [31, 32], which was also used in the past in a collaboration with Tilmann D. Märk, who is honored in this issue of Physica Scripta, to investigate cluster ion-induced electron emission from surfaces [33–36]: In short, electrons emitted from the surface are attracted by a grid ($U_{\mathrm{grid}} = +400$ V) close to the target holder ($U_{\mathrm{holder}} = 0$ V). Additional negative electrodes ensure that the electrons do not escape towards the source ($U_{\mathrm{repeller}} = -150$ V) and do not hit the holder of the grid ($U_{\mathrm{frame}} = -50$ V), respectively. After the grid, the electrons are accelerated onto a passivated implanted planar silicon (PIPS) detector biased at 27 kV. The resulting voltage pulse height is proportional to the number of electrons impinging within the detector dead time and thus gives access to the electron yield, i.e. the number of electrons emitted from the surface per ion impact.

All signals are recorded in coincidence and saved on an event-by-event basis: Per ion reaching the MCP, we thus store the ion exit charge state and scattering angle and the secondary electron yield. The combination of both signals, ion on the MCP and electrons on the PIPS detector, lets us determine the time of flight (TOF) of the ions from the sample to the MCP and corresponds to the energy loss of the ions within the material. This value is

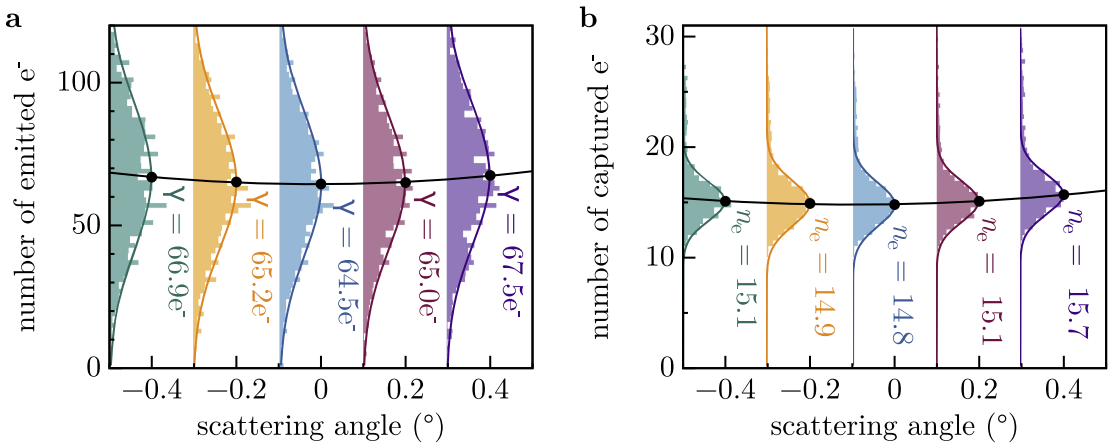

Figure 2. Trajectory-dependent electron statistics spectra (a) and charge exchange distributions (b) for 98 keV Xe^{30+} ions transmitted through graphene. Histograms are shown for five different scattering angle ϕ ranges: $[-0.5°, -0.3°]$ (green), $[-0.3°, -0.1°]$ (orange), $[-0.1°, 0.1°]$ (blue), $[0.1°, 0.3°]$ (red), and $[0.3°, 0.5°]$ (violet). The histograms are plotted on the y-axis and shifted to the ϕ-range start value on the x-axis. The histograms are plotted and the mean values are marked with black dots and labelled with the corresponding mean electron yield γ and mean number of captured electrons n_e. A quadratic fit is added to guide the eye.

important, especially for 2D materials, to distinguish ions transmitted through the 2D layer (small energy loss) from ions transmitted through the support structure (large energy loss) [27]. We consider only data for charge exchange values and small time-of-flight data consistent with values for single-layer graphene [19, 20]. In this way we are able to work with partially contaminated surfaces, where the contaminations lead to a significant separation in ion time-of-flight and charge exchange [27].

All results presented here are TOF-filtered and thus represent the 2D layer without support contribution [29].

Note that while HCIs are, in general, capable of producing pores in 2D materials, this feature is very sensitive to the electronic properties of the material [37]. For graphene, under the applied HCI fluences, no defect formation is expected [19], which significantly differs from experiments performed in the swift heavy ion regime [38, 39].

3. Results

To study the trajectory dependence of electron emission and charge exchange, we split the MCP analysis into five scattering angle regions: $[-0.5°, -0.3°]$, $[-0.3°, -0.1°]$, $[-0.1°, 0.1°]$, $[0.1°, 0.3°]$, and $[0.3°, 0.5°]$. This division is also indicated in figure 1 (top view) in five colors (green, orange, blue, red, violet). Note that even though per definition all scattering angles ϕ are positive, we use here negative and positive ϕ to map the experiment geometry and demonstrate the (expected) measured symmetry. Figure 2 shows the resulting electron yield histograms (a) and exit charge state distributions (b) for transmission of 98 keV Xe^{30+} ions through freestanding single-layer graphene. Coincidences were filtered for the above-specified scattering angle ranges. The histograms are plotted along the y-axes and shifted to the respective angle range start value. For analysis, we fit the histograms with Gaussian distributions and extract the mean electron yield γ and mean exit charge state q, both specified in the graph for each angle range with a black circle and a label.

The minimum electron yield is observed for the central angular angle range (blue), i.e. no or small deflection from the incident direction. A symmetric increase of the mean electron yield with increasing angle is observed, amounting up to +5% for up to 0.5°. This value corresponds well with the increase in transmission time for these deflection angles (see Discussion). A similar trend is present for the mean number of captured electrons: While the minimum $n_e = 14.8$ is recorded for the central window, $n_e > 15$ is found for the two with the largest regarded scattering angle.

The measurement was repeated for the same incident charge state ($q = 30$) but higher kinetic energies. A summary of these results is shown in figure 3, where again the electron yield (a) and the number of captured electrons (b) is depicted. In contrast to figure 2, solely the extracted mean values from Gaussian fits (γ and n_e) are shown. Both data sets for higher energies (116 keV in orange, 130 keV in green) show a similar trend when compared to the data set for 98 keV (red, cf figure 2), i.e. an increase of both γ and n_e with increasing scattering angle. However, absolute values are shifted towards smaller numbers.

Note that the velocity dependence is non-monotonic in figure 3. This might be a result of residual uncertainty in the measurement for different ion parameters (changing ultra-high vacuum pressure conditions,

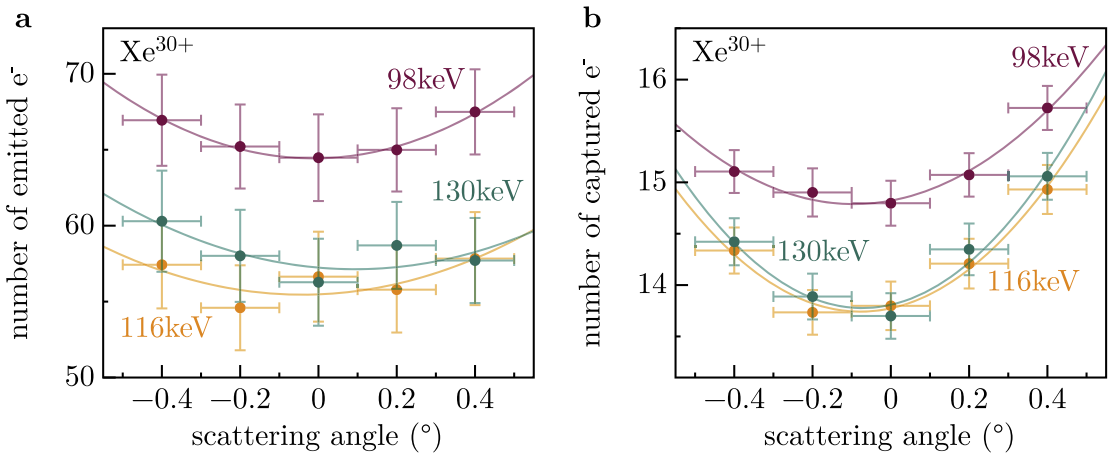

Figure 3. Electron yield (a) and mean number of captured electrons (b) in dependence of the scattering angle for Xe^{30+} projectiles transmitted through graphene with kinetic energies of 98 keV (red), 116 keV (orange), and 130 keV (green). Error bars correspond to the standard deviation σ from the Gaussian fits to the histogram data (cf figure 2). A quadratic fit is added to guide the eye.

MCP noise, TOF-filtering conditions, etc.). Yet, each ion charge and velocity represents a single measurement where the angular information is extracted from the same dataset using different regions-of-interest at the MCP. The angle-dependence follows then from a relative measurement where absolute uncertainties in the captured charge and emitted electron number (in the order of ± 1 electron) cancel out.

4. Discussion

The neutralisation of HCIs is constituted by two factors: At first, the projectile resonantly captures electrons into high-n states, leading to an overall neutral yet still excited particle—a hollow atom (HA) is formed [40, 41]. Following that, the HA deexcites, gradually filling up empty inner shells through radiative and non-radiative processes, with a sizable contribution of ICD being the most efficient and prominent mechanism for HCI-surface interaction [21].

We consider ICD in a broader sense, namely the de-excitation of the incoming neutralising ion in combination with an excitation or ionization of a target atom. We distinguish ICD (two-centre de-excitation) from the preceding resonant charge transfer from the surface feeding electrons into excited states of the ion. Note that off-resonance charge transfer similar to Electronic Transition Mediated Decay (ETMD) may also play a role, but under the condition of above-the-barrier electron capture, the off-resonance energy release is typically smaller than the de-excitation transitions within the ion itself transferring energy via ICD to a target electron.

Polarisation-enhanced Auger-Meitner processes are discussed in literature [42] as a way to explain enhanced non-radiative rates in a single-centre decay. Since Auger-Meitner processes are mediated through electron-electron scattering, any dynamic increase in electron density might increase the probability of Auger-Meitner decay. Time-dependent density functional theory calculations showed that the incoming highly charged ion attracts the target valence electrons (polarises the surface) even before charge transfer sets in [19]. This dynamically formed increased electron density in close proximity of the ion might enhance Auger-Meitner decay within the ion itself. Note that this enhanced electron density is still an external trigger for Auger-Meitner decay while it may or may not be considered a 'two-center' process, where the second centre is then not an atomic nucleus, but rather a spatially distributed electron cloud.

Both processes, HA formation and subsequent deexcitation, happen on different time and length scales. HA formation sets in when the HCI potential overlaps with the material such that the potential barrier becomes smaller than the work function [43]. For Xe^{30+}, this critical distance is reached 22Å above the surface of graphene and is important for the subsequent neutralisation with regard to supplying electrons for stabilisation. By a trajectory length increase of $<0.01\%$ for scattering angles of $0.5°$ compared to a straight path, the HA formation does not benefit from increasing scattering. ICD, on the flip side, is very sensitive to the distance between the HCI and material atoms and most-efficient at distances $r < 1.4\,\mathring{A}$ [20, 44]. At large separations, ICD rates decrease as $1/r^6$, which makes ICD significant only in the closest proximity of the material layer. When the ion leaves the efficient deexcitation region around the material layer, only radiative and single-centre (intra-atomic) Auger-Meitner processes can continue to contribute to the ion deexcitation.

As depicted in figure 3, the electron yield and number of captured electrons show a clear trend towards increasing values by approximately +5% when the scattering angle increases from $\phi = 0°$ to $\phi = 0.5°$. Scattering-angle-dependent charge exchange was already found for transmission experiments with graphene [25] and increasing electron yields in grazing scattering experiments with bulk samples [24]. In both cases, larger angle ranges were considered and Creutzburg *et al* discussed for the same experimental geometry as here a quadratic dependency of the charge exchange with angles up to $\phi = 2°$ [25]. Our small increase in electron yield of ∼5% is a result of the small angular range covered by our MCP detector. The quadratic yield increase with angle lets us expect a relative electron yield increase of ∼60% for larger scattering of for example $\phi = 2°$.

Unlike thicker multi-layer materials, where multiple scattering hides a direct link between scattering angle and impact parameter [25], for free-standing graphene, the current experiment exploits the true single-scattering regime. In principle, one can link the scattering angle to the impact position of the collision within the graphene hexagon lattice. However, a quantitative analysis is non-trivial because it requires accurate knowledge of the scattering potential for the complex collision system involving a partially screened HA and a dynamic charge density evolution in the surface [23].

There is also a kinetic energy trend observed in figure 3. Compared to the 98 keV data shown in figure 2 and 3, both other data sets in figure 3 with higher kinetic energies show less neutralisation behaviour: smaller secondary electron yields and smaller numbers of captured electrons. This result is consistent with previous measurements showing that the potential energy deposition (i.e. neutralisation) depends on the particle velocity and overall interaction time with the sample layer [19, 20]. Overall, data for the electron statistics scatters much more than data points for the charge exchange. This is due to different detector resolutions in our setup for both measured quantities [29].

The trajectory dependence obvious in figure 3 can stem, e.g. from the following two contributions (or convolutions thereof): For interatomic processes (1) like ICD, which has lifetimes on the order of the interaction time and is efficient only at small interatomic separations, a smaller distance of closest approach and an extended interaction time (due to an increased trajectory length upon deflection) could already explain an enhanced neutralisation for larger scattering angles. Similarly, (2) a dynamic increase of the electron density at the impact point due to polarisation from the large positive Coulomb charge of the ion might enhance two-centre Auger-Meitner rates further and may therefore also benefit from smaller interatomic distances.

From the present data, we cannot unambiguously determine which of the two above-mentioned processes cause(s) the trajectory-dependent neutralisation, i.e. if it is the ICD-distance dependence alone or if polarization-enhancement is an important additional ingredient. Further experiments are necessary to unravel neutralisation of ions *inside* material surfaces and particle emission from the materials. To study individual atom scattering like in the gas phase, but coupled to a virtually infinite electron reservoir, we suggest to repeat the study discussed here with a graphene layer decorated with a low density of dispersed Au atoms. Carbon atoms limit the maximum scattering angle of Xe to $\phi = 5.34°$. For the heavier Au atoms, larger scattering angles are possible. Recording data for $\phi > 5.34°$ can then be attributed to scattering from individual Au atoms and the distance of minimal approach can be calculated. This allows for a more direct determination of the trajectory and paves the way for accompanying simulations for the extracted flight path. Implanting three-fold coordinated Au atoms into free-standing graphene was already demonstrated by Trentino *et al* [45].

5. Conclusion

Our scattering-angle-resolved data of HCI charge exchange and secondary electron emission upon transmission through single-layer graphene clearly shows that the neutralisation of the particle depends on the trajectory within the material: As scattering angles increase, so does the neutralization efficiency as well as the number of emitted electrons. This implies that processes, which are enhanced in the vicinity of sample atoms, contribute significantly to the deexcitation, like interatomic Coulombic decay or polarisation-enhanced Auger-Meitner processes. Future experiments using alternative target materials, such as Au-decorated graphene, are suggested which would allow to investigate the effects of varying scattering angles in more detail.

Acknowledgments

We thank Filip Vuković for fruitful discussions. This research was funded in whole or in part by the Austrian Science Fund (FWF) [10.55776/Y1174, 10.55776/P36264, and 10.55776/I4914]. For open access purposes, the author has applied a CC BY public copyright license to any author accepted manuscript version arising from this submission.

Data availability statement

The data cannot be made publicly available upon publication because they are not available in a format that is sufficiently accessible or reusable by other researchers. The data that support the findings of this study are available upon reasonable request from the authors.

ORCID iDs

A Niggas https://orcid.org/0000-0002-5838-5789
F Aumayr https://orcid.org/0000-0002-9788-0934
R A Wilhelm https://orcid.org/0000-0001-9451-5440

References

[1] Gillaspy J D 2001 Highly charged ions *J. Phys. B: At. Mol. Opt. Phys.* **34** R93
[2] DREEBIT | Ion Beam Technology. Ionisation Energy Database. https://dreebit-ibt.com/ionization-energy-database.html, 2023.
[3] Scheers J *et al* 2020 EUV spectroscopy of highly charged Sn 13 + Sn 15 + ions in an electron-beam ion trap *Phys. Rev.* A **101** 062511
[4] Versolato O O 2019 Physics of laser-driven tin plasma sources of EUV radiation for nanolithography *Plasma Sources Sci. Technol.* **28** 083001
[5] Torretti F *et al* 2020 Prominent radiative contributions from multiply-excited states in laser-produced tin plasma for nanolithography *Nat. Commun.* **11** 2334
[6] King S A *et al* 2022 An optical atomic clock based on a highly charged ion *Nature* **611** 43–7
[7] Kozlov M G, Safronova M S, Crespo López-Urrutia J R and Schmidt P O 2018 Highly charged ions: optical clocks and applications in fundamental physics *Rev. Mod. Phys.* **90** 045005
[8] Barat M, Gaboriaud M N, Guillemot L, Roncin P, Laurent H and Andriamonje S 1987 Coincident energy gain spectroscopy of electron capture in multiply charged ions colliding with He, H_2 and heavy rare-gas targets *J. Phys. B: At. Mol. Phys.* **20** 5771–83
[9] Stolterfoht N, Platten H, Schiwietz G, Schneider D, Gulyás L, Fainstein P D and Salin A 1995 Two-center electron emission in collisions of fast, highly charged ions with He: experiment and theory *Phys. Rev.* A **52** 3796–802
[10] Schenkel T, Hamza A V, Barnes A V and Schneider D H 1999 Interaction of slow, very highly charged ions with surfaces *Prog. Surf. Sci.* **61** 23–84
[11] Rothard H, Lanzanò G, Gervais B, De Filippo E, Caron M and Beuve M 2015 Swift heavy ion induced electron emission from solids *J. Phys. Conf. Ser.* **629** 012007
[12] Rothard H, Kroneberger K, Clouvas A, Veje E, Lorenzen P, Keller N, Kemmler J, Meckbach W and Groeneveld K-O 1990 Secondary-electron yields from thin foils: a possible probe for the electronic stopping power of heavy ions *Phys. Rev.* A **41** 2521–35
[13] Aumayr F, Facsko S, El-Said A S, Trautmann C and Schleberger M 2011 Single ion induced surface nanostructures: a comparison between slow highly charged and swift heavy ions *J. Phys. Condens. Matter* **23** 393001
[14] El-Said A S *et al* 2008 Creation of nanohillocks on CaF 2 surfaces by single slow highly charged ions *Phys. Rev. Lett.* **100** 237601
[15] Heller R, Facsko S, Wilhelm R A and Möller W 2008 Defect mediated desorption of the KBr(001) surface induced by single highly charged ion impact *Phys. Rev. Lett.* **101** 096102
[16] Winecki S, Cocke C L, Fry D and Stöckli M P 1996 Neutralization and equilibration of highly charged argon ions at grazing incidence on a graphite surface *Phys. Rev.* A **53** 4228–37
[17] Hattass M, Schenkel T, Hamza A V, Barnes A V, Newman M W, McDonald J W, Niedermayr T R, Machicoane G A and Schneider D H 1999 Charge equilibration time of slow, highly charged ions in solids *Phys. Rev. Lett.* **82** 4795–8
[18] Herrmann R, Cocke C L, Ullrich J, Hagmann S, Stoeckli M and Schmidt-Boecking H 1994 Charge-state equilibration length of a highly charged ion inside a carbon solid *Phys. Rev.* A **50** 1435–44
[19] Gruber E *et al* 2016 Ultrafast electronic response of graphene to a strong and localized electric field *Nat. Commun.* **7** 13948
[20] Niggas A *et al* 2021 Peeling graphite layer by layer reveals the charge exchange dynamics of ions inside a solid *Communications Physics* **4** 180
[21] Wilhelm R A, Gruber E, Schwestka J, Kozubek R, Madeira T I, Marques J P, Kobus J, Krasheninnikov A V, Schleberger M and Aumayr F 2017 Interatomic coulombic decay: the mechanism for rapid deexcitation of hollow atoms *Phys. Rev. Lett.* **119** 103401
[22] Jahnke T 2015 Interatomic and intermolecular Coulombic decay: the coming of age story *J. Phys. B: At. Mol. Opt. Phys.* **48** 082001
[23] Niggas A *et al* 2022 Ion-induced surface charge dynamics in freestanding monolayers of graphene and MoS 2 probed by the emission of electrons *Phys. Rev. Lett.* **129** 086802
[24] Lemell C, Stöckl J, Burgdörfer J, Betz G, Winter H P and Aumayr F 2000 Coincidence measurements of highly charged ions interacting with surfaces *AIP Conference Proceedings* **500** 656–65 AIP
[25] Creutzburg S, Niggas A, Weichselbaum D, Grande P L, Aumayr F and Wilhelm R A 2021 Angle-dependent charge exchange and energy loss of slow highly charged ions in freestanding graphene *Phys. Rev.* A **104** 042806
[26] Graphenea. Graphene on TEM grids. https://www.graphenea.com, 2024.
[27] Niggas A, Schwestka J, Creutzburg S, Gupta T, Eder D, Bayer B C, Aumayr F and Wilhelm R A 2020 The role of contaminations in ion beam spectroscopy with freestanding 2D materials: a study on thermal treatment *J. Chem. Phys.* **153** 014702
[28] Schwestka J, Melinc D, Heller R, Niggas A, Leonhartsberger L, Winter H, Facsko S, Aumayr F and Wilhelm R A 2018 A versatile ion beam spectrometer for studies of ion interaction with 2D materials *Rev. Sci. Instrum.* **89** 085101
[29] Niggas A, Schwestka J, Weichselbaum D, Heller R, Aumayr F and Wilhelm R A 2022 Coincidence technique to study ion-induced electron emission from atomically thin materials *Proc. SPIE* **12131, Nanophotonics IX** 121310H SPIE
[30] RoentDek Handels GmbH. CoboldPC Software. http://roentdek.com/, 2018. Publisher: http://roentdek.com/.
[31] Aumayr F, Lakits G and Winter H 1991 On the measurement of statistics for particle-induced electron emission from a clean metal surface *Appl. Surf. Sci.* **47** 139–47
[32] Lakits G, Aumayr F and Winter H 1989 Statistics of ion-induced electron emission from a clean metal surface *Rev. Sci. Instrum.* **60** 3151–9

[33] Aumayr F, Märk T D and Winter H 1993 The statistics of electron emission from clean metal surfaces induced by slow ions: measurement and recent applications *Int. J. Mass Spectrom. Ion Process.* **129** 17–29
[34] Vana M, Aumayr F, Winter H P, Drexel H, Grill V, Scheier P and Märk T D 1997 Electron emission for impact of slow fullerene ions on clean gold *Phys. Scr.* T **73** 318–9
[35] Winter H P, Vana M, Betz G, Aumayr F, Drexel H, Scheier P and Märk T D 1997 Suppression of potential electron emission for impact of slow multicharged fullerenes on clean gold *Phys. Rev.* A **56** 3007–10
[36] Aumayr F, Betz G, Märk T D, Scheier P and Winter H P 1998 Electron emission from a clean gold surface bombarded by slow multiply charged fullerenes *Int. J. Mass Spectrom. Ion Process.* **174** 317–28
[37] Grossek A S, Niggas A, Wilhelm R A, Aumayr F and Lemell C 2022 Model for nanopore formation in two-dimensional materials by impact of highly charged ions *Nano Lett.* **22** 9679–84
[38] Nebogatikova N A, Antonova I V, Erohin S V, Kvashnin D G, Olejniczak A, Volodin V A, Skuratov A V, Krasheninnikov A V, Sorokin P B and Chernozatonskii L A 2018 Nanostructuring few-layer graphene films with swift heavy ions for electronic application: tuning of electronic and transport properties *Nanoscale* **10** 14499–509
[39] Nebogatikova N A, Antonova I V, Gutakovskii A K, Smovzh D V, Volodin V A and Sorokin P B 2023 Visualization of swift ion tracks in suspended local diamondized few-layer graphene *Materials* **16** 1391
[40] Briand J P, de Billy L, Charles P, Essabaa S, Briand P, Geller R, Desclaux J P, Bliman S and Ristori C 1990 Production of hollow atoms by the excitation of highly charged ions in interaction with a metallic surface *Phys. Rev. Lett.* **65** 159
[41] Winter H and Aumayr F 1999 Hollow atoms *J. Phys. B: At. Mol. Opt. Phys.* **32** R39–39
[42] Deutscher S A, Díez Muiño R, Arnau A, Salin A and Zaremba E 2001 Distorted wave approach to calculate Auger transition rates of ions in metals *Nucl. Instrum. Methods Phys. Res., Sect. B* **182** 8–14
[43] Burgdörfer J, Lerner P and Meyer F W 1991 Above-surface neutralization of highly charged ions: the classical over-the-barrier model *Phys. Rev.* A **44** 5674–85
[44] Wilhelm R A and Grande P L 2019 Unraveling energy loss processes of low energy heavy ions in 2D materials *Communications Physics* **2** 89
[45] Trentino A, Mizohata K, Zagler G, Längle M, Mustonen K, Susi T, Kotakoski J and Åhlgren E H 2022 Two-step implantation of gold into graphene *2D Materials* **9** 025011